OPEN ACCESS
IOP Publishing
Nanotechnology
Nanotechnology **34** (2023) 145601 (8pp)
https://doi.org/10.1088/1361-6528/acabd1

Effect of surface gallium termination on the formation and emission energy of an InGaAs wetting layer during the growth of InGaAs quantum dots by droplet epitaxy

D Fricker[1,2,*], P Atkinson[3], X Jin[1,2], M Lepsa[1,4], Z Zeng[1,2], A Kovács[5], L Kibkalo[5], RE Dunin-Borkowski[2,5] and BE Kardynał[1,2,*]

[1] Peter Grünberg Institute 9, Forschungszentrum Jülich, D-52425 Jülich, Germany
[2] Department of Physics, RWTH Aachen University, D-52074 Aachen, Germany
[3] Institut des Nano Sciences de Paris, CNRS UMR 7588, Sorbonne Université, F-75005 Paris, France
[4] Peter Grünberg Institute 10, Forschungszentrum Jülich, D-52425 Jülich, Germany
[5] Ernst Ruska-Centre for Microscopy and Spectroscopy with Electrons, Peter Grünberg Institute 5, Forschungszentrum Jülich, D-52428 Jülich, Germany

E-mail: d.fricker@fz-juelich.de and b.kardynal@fz-juelich.de

Received 30 June 2022, revised 17 November 2022
Accepted for publication 14 December 2022
Published 23 January 2023

Abstract

Self-assembled quantum dots (QDs) based on III–V semiconductors have excellent properties for applications in quantum optics. However, the presence of a 2D wetting layer (WL) which forms during the Stranski–Krastanov growth of QDs can limit their performance. Here, we investigate WL formation during QD growth by the droplet epitaxy technique. We use a combination of photoluminescence excitation spectroscopy, lifetime measurements, and transmission electron microscopy to identify the presence of an InGaAs WL in these droplet epitaxy QDs, even in the absence of distinguishable WL luminescence. We observe that increasing the amount of Ga deposited on a GaAs (100) surface prior to the growth of InGaAs QDs leads to a significant reduction in the emission wavelength of the WL to the point where it can no longer be distinguished from the GaAs acceptor peak emission in photoluminescence measurements. However increasing the amount of Ga deposited does not suppress the formation of a WL under the growth conditions used here.

Keywords: droplet epitaxy, InAs/GaAs, wetting layer properties, wetting layer characterization

(Some figures may appear in colour only in the online journal)

1. Introduction

The study of epitaxial semiconductor quantum dots (QDs) as a platform for non-classical light sources has been driven by growing interest in quantum communication. Single photon emission of InAs/Ga(Al)As QDs grown by molecular beam epitaxy (MBE) was first reported in 2001 [1]. These QDs were grown in the Stranski–Krastanov (SK) growth mode, in which QD formation is driven by strain relaxation of the InAs layer when the layer thickness exceeds a critical thickness resulting in QDs sitting on top of a thin (<1.5 monolayer) wetting layer (WL) [2].

The optical properties of SK QDs have been extensively studied and used to create single photon, indistinguishable and entangled photon light sources for quantum communication [3, 4]. One, inherent disadvantage of the SK growth mode is the presence of a WL. This WL has a strong effect on carrier dynamics [5] and can provide a pathway for carrier escape from

* Authors to whom any correspondence should be addressed.

QDs if the energetic separation between QDs and WL is small leading to thermal quenching of QD luminescence [6].

In addition, the presence of carriers in the WL is a source of decoherence leading to strong damping of Rabi oscillations during optical manipulation of excitonic qubits limiting their applicability for quantum computation applications [7, 8] leading for example to decoherence processes in the QDs that are highly undesired in some applications [6, 7, 9].

For SK-grown QDs, it is possible to remove the confined electronic states in the WL conduction band by the use of an AlAs capping layer [9] thus potentially avoiding many of the negative consequences of a WL on the QD emission properties. However there still remain two-dimensional confined hole states in the WL valence band in this case.

In this work we study an alternative QD growth technique, droplet epitaxy (DE), that has been previously reported to result in wetting-layer free QDs for both InAs/GaAs QDs [10] and GaAs/AlGaAs QDs [11]. Droplet epitaxy consists of the deposition of a group III metal in the absence of the group V flux at relatively low substrate temperatures (typically $<350\,^{\circ}\mathrm{C}$). The group III metal forms droplets on the surface that are subsequently recrystallized by exposure to the group V flux. After capping and suitable annealing of these QDs, their optical properties have been shown to be comparable to SK-grown QDs [12, 13].

The growth of GaAs QDs on AlGaAs surfaces has been well studied in the literature. At low enough group temperatures ($\sim$180 °C for Ga droplets) and high enough group V fluxes, the dots remain well defined and outdiffusion from the droplets to the neighboring surface is limited, preventing the formation of a WL [11]. In contrast, at higher temperatures ($\geqslant$300 °C for Ga droplets) clear outdiffusion occurs from the droplets leading to a 2D GaAs ring around the dot [14]. However, the growth of InAs dots on GaAs by droplet epitaxy has been less extensively studied and the growth window for the formation of wetting-layer free QDs has not been determined [10]. Monte Carlo simulations of the In deposition on an As-terminated GaAs surface indicate that a WL of a single monolayer, with one In atom binding to the As on the As-terminated GaAs surface will always occur [15] indicating that the surface termination of the GaAs surface prior to In deposition is crucial.

In this report, we study the effect of the Ga amount used to prepare a Ga-terminated surface, prior to the droplet epitaxy of In(Ga)As dots, on the emission wavelength of the WL. We study WL electronic states using photoluminescence excitation (PLE) and time-resolved photoluminescence (TR PL), both of which reveal the presence of a WL even when the WL emission cannot be clearly identified in photoluminescence (PL) spectroscopy. The In distribution in the WLs grown on different Ga-terminated surfaces is studied using transmission electron microscopy (TEM). We conclude that despite growth conditions that are expected to result in a Ga-terminated surface, this is insufficient to suppress the formation of a WL.

2. Epitaxy

The investigated samples were grown on undoped (100) GaAs substrates in a molecular beam epitaxy system from MBE Komponenten, using an arsenic valve cracker cell for As_4 flux control and a pyrometer to measure the substrate temperature. After thermal deoxidation of the substrate, a buffer layer consisting of 295 nm GaAs followed by 30 pairs of a GaAs/AlAs (1 nm/3 nm) smoothing superlattice, followed by 205 nm GaAs, was grown. The substrate temperature was 630 °C and the GaAs (AlAs) growth rate was 1 (0.33) monolayer(ML)/s respectively. The As:Ga b.e.p. ratio during the buffer growth was 27.

At the end of the buffer layer growth the substrate temperature was reduced to 575 °C. The As_4 valve was then closed. After 5 min at 575 °C, the substrate was cooled to 350 °C over 20 min, both steps allowing the residual arsenic in the chamber to be pumped away. When the chamber background pressure reached 8×10^{-9} mbar, 1.8 ML of Ga was deposited on the GaAs surface, which should result in a Ga-terminated GaAs surface [11, 16, 17]. On this surface 1.4 ML of In was then deposited to form In droplets. The Ga growth rate used here was 0.06 ML s^{-1}, and the In growth rate used was 0.045 ML s^{-1}. The growth rates and the Ga and In layer thicknesses given are those of the equivalent GaAs and InAs growth rates and thicknesses if the layers were grown under an As overpressure.

The droplets were immediately crystallized with an As_4 beam flux of 2×10^{-5} mbar to form InGaAs QDs. Simultaneously, slow heating of the wafer was started. After 30 min, when the substrate temperature reached 530 °C the QDs were capped with a 2 nm thick GaAs layer, followed by a 10 min growth interruption during which the substrate temperature was raised to 580 °C. This partial cap and higher temperature anneal limits the height of the dots and hence the PL emission wavelength [18]. Finally, the structure was completed with a growth of a 98 nm thick GaAs layer at 580 °C. The cap layers were grown with a GaAs growth rate of 1 ML s^{-1}.

The deposition amounts given here (1.8 ML Ga, 1.4 ML In) are given for the wafer centre. However, the Ga and In deposition steps were performed without wafer rotation, resulting in a variation in the deposition amount across a 4 inch wafer. Based on simulations by the manufacturer MBE Komponenten, the variation is expected to be $\pm 25\,\%$. After the Ga deposition step the substrate azimuthal direction was changed to ensure that the In flux gradient was orthogonal to the Ga flux gradient. This method permits the effect of the Ga deposition amount to be studied in a single sample, which has the advantage that all other growth parameters should be identical.

It is however known that there is a small radial temperature variation across a substrate. To check whether this temperature variation could be the cause of the changes in WL and QD PL observed across the substrate, a second wafer with a different Ga deposition amount was also studied. This second wafer, grown under nominally identical growth conditions as the first wafer, had a Ga amount at the wafer centre of 2.16 ML. Regions with the same Ga and In deposition amount on each wafer therefore occur at different radial positions and hence slightly different temperatures. Comparison of the PL from these 2 wafers, as discussed later, show that a temperature gradient across the substrate cannot

account for the shift in emission wavelength observed, but is clearly correlated to the change in Ga deposition amount.

3. Sample characterization

3.1. Optical characterization

Mapping of the PL across the wafer was carried out with meV resolution, using a cold finger He cryostat mounted on a manual stage allowing large movements of the sample. The nominal sample temperature on the cold finger is 4 K.

More detailed μ-PL, PLE and TR PL measurements were carried out in a closed-cycle cryostat, where the samples were mounted on a computer-controlled *xyz*-stage offering sub-μm resolution. The sample temperature was in this case 1.5 K. An achromatic lens with a numerical aperture (NA) of 0.81 focused the laser beam on the sample and collected the resulting PL signal. A continuous wave (CW) Ti:sapphire laser with a tunable wavelength was used to perform the μ-PL and PLE measurements.

To perform the TR PL measurements, a pulsed diode laser with a tuneable pulse repetition rate up to 80 MHz and an emission wavelength of 660 nm was used. The laser pulse width was ∼200 ps. The emitted PL was spectrally selected with wavelength-tunable filters and guided to a single-photon avalanche photodiode, which has 30 ps time resolution.

3.2. Structural characterization

Structural characterization of uncapped QDs was carried out using an atomic force microscope (AFM) in tapping mode to scan the sample surface with sub nm precision. Further, high-angle annular dark-field (HAADF) scanning TEM (STEM) imaging was used to gain insight into the InGaAs layer after capping. Cross-sectional specimens were prepared using focused Ga ion beam (FIB) sputtering in a dual beam scanning electron microscope. The surface damage was reduced by low-energy (<1 keV) Ar ion beam sputtering [19]. The HAADF images were recorded using an electron probe aberration corrected microscope operated at 200 kV [20]. The inner annular dark-field detector semi-angle used was 69 mrad, resulting in HAADF imaging, which is sensitive to chemical composition as the image intensity scales approximately as $I \sim Z^2$, where Z is the atomic number of an atom involved in an electron scattering ($Z_{In} = 49$, $Z_{Ga} = 31$).

4. Results and discussion

Figure 1(a) shows normalized μ-PL spectra obtained at different positions on wafer 1 along the Ga gradient. The positions correspond to Ga amounts of 1.4 ML, 1.8 ML and 2.2 ML. The deposited In amount was 1.4 ML. The two PL peaks at 818 and 830 nm, present in all three spectra, originate from radiative recombination of the GaAs free exciton and the free electron-neutral acceptor, (A^0, e), respectively [21, 22]. The positions of these GaAs PL lines are, as expected, independent of the Ga amount deposited during the Ga-termination step.

The emission wavelength of the WL peak decreases from ∼845 to ∼834 nm as the Ga deposition amount is increased from 1.4 to 1.8 ML. At 2.2 ML Ga deposition amount, the WL emission can no longer be resolved from the tail of the GaAs (A^0, e) peak in the PL spectrum.

PL measurements in fine steps along the Ga gradient track the development of the WL emission wavelength with Ga amount in more detail. The spectra shown in figure 1(b) were recorded in 1 mm steps along the Ga-gradient on wafer 1. Each spectrum in figure 1(b) was fitted with one Gaussian function for the WL emission peak. When the WL and (A^0, e) emission peaks overlapped, fitting included a second Gaussian function fixed at (A^0, e). The central wavelengths of the fitted functions for the WL are plotted as black points in figure 1(c). The position on the wafer is converted into the expected amount of Ga using the model provided by the manufacturer of the used MBE system. The WL emission wavelength continuously decreases from 847 to 834 nm, with the Ga amount increasing from 1.35 to 1.85 ML. It then remains constant until the WL can no longer be resolved at ∼2.15 ML of Ga.

For this measurement, the wafer was cut into smaller strips that would fit simultaneously onto the cold finger of the cryostat. Abrupt changes of the WL emission wavelength, visible at ∼1.45 ML, ∼1.6 ML and ∼1.85 ML, correspond to the points at which a different piece of the wafer is measured. These jumps in wavelength are most likely due to small offsets in the measurement temperature of different pieces. On repeating the measurements with sample placed at different positions on the cold finger, variations in the WL emission of up to 0.8 nm were observed. These fluctuations were not observed in the measurements with good temperature control which are discussed below.

The central wavelength of WL emission on wafer 2 is shown in red in figure 1(c) and shows a similar small variation in WL emission energy with increasing Ga deposition amount. There is a good overlap of the WL emission for wafers 1 and 2 for the Ga deposition amount between 1.9 and 2.1 ML, despite the fact that these Ga deposition amounts occur at different spatial positions on the two wafers i.e. near the edge of one wafer and the centre of the other. This means that any effect of a difference in substrate temperature from centre to edge of the wafer can be neglected, and only the effect of the Ga deposition amount on WL formation is considered in the following discussion.

Further insight into the growth can be gained from looking at the photoluminescence of the QDs and at AFM images of the surface after the QD deposition step. Figure 1(d) shows μ-PL spectra taken at the same positions as the spectra shown in 1(a). Figures 1(e)–(g) shows corresponding AFM images of the surface after the Ga and In deposition and surface anneal under arsenic, using the same growth conditions as described previously.

A broad PL signal, indicating a high QD density is observed from the 1.4 and 2.2 ML Ga regions. In contrast, emission from isolated QDs is observed in the sample with

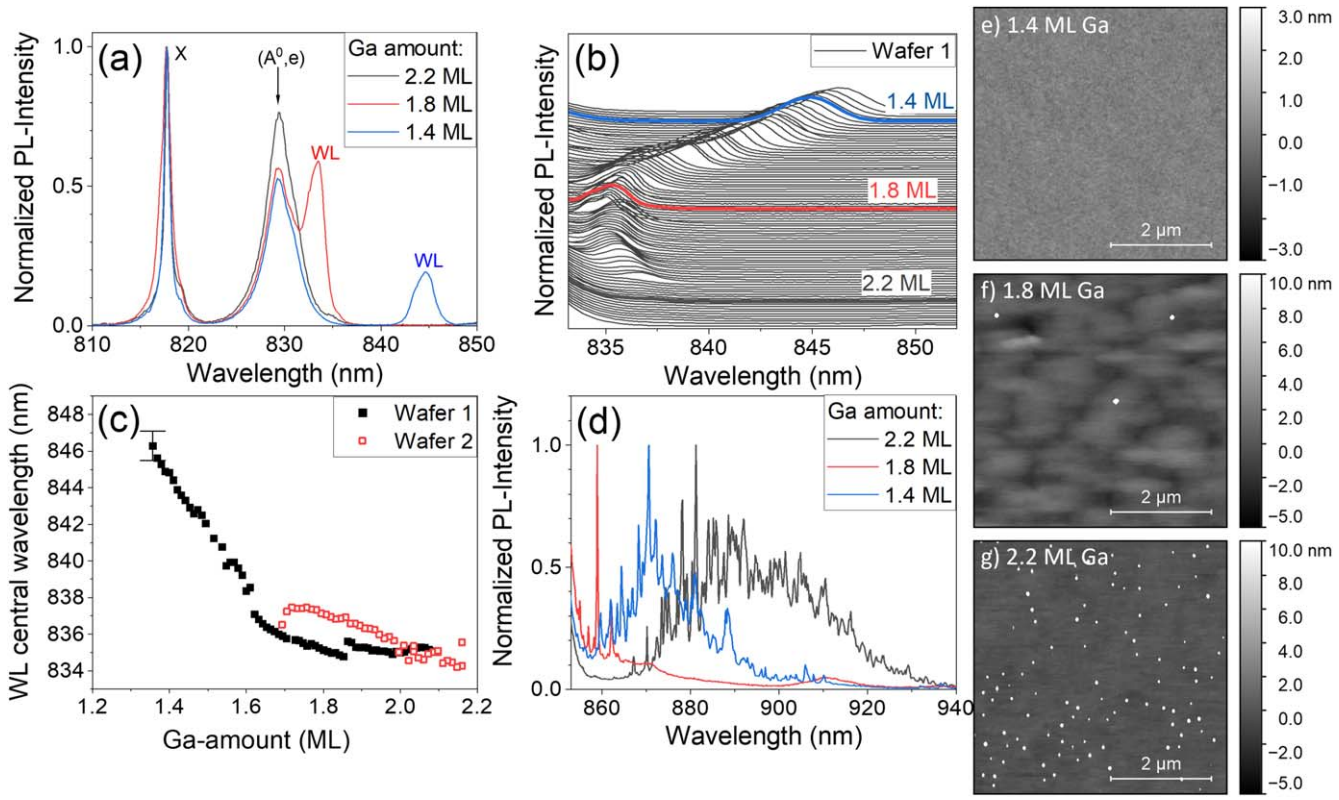

Figure 1. (a) Normalized μ-PL spectras showing the GaAs and WL emission from three different positions on wafer 1 along the Ga gradient. (b) Normalized wetting layer signal measured on wafer 1 along the Ga gradient in 1 mm steps. (c) Central wavelength of the Gaussian function fitted to the signal assigned to wetting layer emission for wafers 1 and 2. Wafer 1 had a deposition of 1.8 ML Ga at the wafer centre, while wafer 2 had a deposition of 2.16 ML Ga at the centre. Both wafers had the same deposition amount of In (1.4 ML) at the centre. Small differences in the measurement temperature of each sample cut from wafer 1 results in abrupt changes in the WL emission wavelength at $\sim$1.45, $\sim$1.6 and $\sim$1.85\,ML of Ga. (d) Normalized μ-PL spectra showing the QD emission from the same positions on wafer 1 as in (a). (e)–(f) AFM scans from three different positions of uncapped QDs grown under the same conditions as the QDs from wafer 1 along the Ga gradient. Note the different height scales of the AFM images.

1.8 ML Ga deposition. The dot density in this case is $\sim 10^5$ QDs cm^{-2} as estimated by μ-PL maps of several 100 μm^2 areas.

For 1.4 ML Ga deposition, dots are not visible on the surface. The AFM scan shows an RMS height fluctuation of 0.2 nm and a maximum step size of 0.6–0.9 nm, corresponding to 2–3 ML thickness variations in the material. In PL, a strong WL signal is seen but there is additional QD emission observed at 40 ± 15 meV from the WL peak. These dots are believed to be natural InAs/GaAs QDs that form in the WL due to fluctuations in the In composition and thickness of the WL [23, 24] similar to the natural dots that form in thin disordered GaAs/AlAs QWs [25, 26].

The energy separation between WL and natural dots that we observe in figure 1 is greater than the $\sim$20 meV confinement previously reported in WL natural QDs [23, 24]. This may be due to the difference between the SK growth mode and the DE growth mode. In the SK growth mode, the initial growth of InAs on GaAs is layer-by-layer i.e. resulting in complete wetting of the surface. In contrast, in the DE growth mode the In which is initially deposited in the absence of As may not uniformly wet the surface depending on the surface termination condition. Therefore, after recrystallization and capping, the WL that forms in the DE mode may have larger In composition fluctuations than in the SK mode. Alternatively, the larger confinement observed in these natural QDs may also be due to the long growth interruption in our case ($\sim$30 mins) prior to capping of the recrystallized InAs.μ

In the region with 1.8 ML Ga deposition, a low density of dots, $\sim$0.1 QDs μm^{-2}, can be observed in the AFM scan. This density increases to $\sim$4 QDs μm^{-2} for 2.2 ML Ga deposition. This agrees well with the μ-PL spectra which show a low dot density in the 1.8 ML Ga region and the high dot density in the 2.2 ML Ga region.

The change in InAs dot density with Ga deposition amount can be understood as follows. On an arsenic-terminated surface, the first 0.75–1.75 ML of the group III deposition will bond to the excess arsenic on the surface, forming a WL and droplet formation only starts to occur once the surface is metal-rich [11]. This is consistent with the AFM and μ-PL measurements in figures 1(d)–(g) in which it can be seen that at 1.4 ML Ga deposition, when the surface is not completely Ga-terminated, In deposition leads to a flat WL, with composition fluctuation natural QDs. InAs QDs only start forming at $\sim$1.8 ML Ga deposition i.e. close to where it is expected that the surface is Ga-terminated. It should be noted that the amount of Ga needed to terminate the surface

depends also on the residual arsenic overpressure in the chamber and so is not well defined. In our case it is likely that the surface is not fully Ga-terminated after ∼1.8 ML Ga deposition and some of the 1.4 ML In deposited will be consumed in bonding to the remaining excess arsenic on the surface prior to droplet formation. This is consistent with the presence of a WL signal in PL at ∼1.8 ML Ga deposition. Increasing the Ga deposition will reduce the amount of excess arsenic on the surface and therefore will lead to an increase in the InAs dot density since more of the In deposited will be available to form droplets. This is consistent with the change in the AFM and QD PL from 1.8 to 2.2 ML Ga deposition. At some threshold Ga value, we would expect also to form Ga droplets on the surface, but this has not been investigated here.

When the Ga deposition is ∼2.1 ML we do not see PL from a WL. We consider three possible explanations for the absence of this WL signal. Firstly, it is possible that that the formation of the WL has been completely suppressed by the Ga deposition above ∼2.1 ML. This would mean that the surface reconstruction is fully Ga-terminated by 2.2 ML deposition and that all the In deposited forms droplets and does not wet the surface at all.

A second possible explanation for the missing WL PL peak is that the WL emission persists but overlaps with the acceptor signal, so that differentiation in PL measurements is not possible for samples with more than 2.2 ML of deposited Ga. The two PL signals can however be distinguished by time-resolved PL, if WL and acceptor-mediated PL occur with different decay times.

The third possible explanation for the absence of the WL PL signal is that there is rapid relaxation of photo-excited carriers from the WL into the QDs, so that PL signal from the WL is not observable. The presence of a WL in the latter case can be probed using PLE.

4.1. PLE

PLE measurements were performed with a wavelength-tunable Ti:Sapphire laser in the μ-PL set-up. Representative PLE data are shown for samples with different Ga amounts in figures 2(a)–(c). The data represent the QD emission intensity as a function of excitation wavelength. The spectra are normalized to the maximum signal. Figure 2(d) shows the PL spectra acquired with an excitation wavelength of 780 nm for the three regions measured by PLE. Since these wafer regions feature high density of QDs, a signal from several QDs is seen in figure 2(d). The QD emission wavelength ranges from 855 to 950 nm and depends on the deposited Ga amount as shown in figure 1(d). No significant differences were observed in the PLE spectra for the different dots measured, so PLE data is shown for a single representative QD with its PL in the inset.

Figure 2(a) shows the data for 1.4 ML of deposited Ga amount from wafer 1. The PLE data demonstrate a clear increase in QD intensity when the laser light is resonant with the GaAs optical bandgap at 818 nm and with the WL states. Excitation of both the light hole WL_{LH} and the heavy hole WL_{HH} WL states contributes to the PL from the QDs [27]. The WL_{HH} state is also observable in PL measurements and there is a Stokes shift of 2 nm (3.5 meV) between the PLE and PL peak positions. Figure 2(b) shows the data for 2.2 ML of Ga from wafer 2. For 2.2 ML, the PL from WL emission at a wavelength of 833 nm partially overlaps with the (A^0, e) signal, which can be seen from fitting with two Gaussian functions. Both, the Stokes shift between the PL and PLE signal of the WL_{HH} states and the wavelength difference between heavy and light hole WL states decreases with the wavelength of the PLE WL_{HH} signal (compare figures 2(a) and (b)), probably as a result of weaker confinement of the different states within the WL.

The 2.6 ML sample does not show a detectable WL in the PL spectrum but the PLE data nevertheless show a clear evidence of the WL presence in figure 2(c). The positions of WL_{HH} and WL_{LH} in figures 2(b) and (c) are very close to each other with ∼824–825 nm and ∼833–834 nm, respectively, despite different amount of the deposited Ga.

Other PLE measurements on wafers 1 and 2 at positions with different WL wavelengths show the same effect as that presented here. The presence of the WL means that the Ga deposition did not prevent In from incorporating into the layer. Since the electronic states in the WL ($\mathrm{WL_{HH}}$ and $\mathrm{WL_{LH}}$) are very close for 2.2 and 2.6 ML of Ga, the composition and thickness of the two WLs are most likely very similar as well.

4.2. TR PL

Time-resolved photoluminescence measurements were performed in the μ-PL set-up using a pulsed diode laser. Figure 3 shows lifetime measurements on two samples with different Ga amounts: a 1.4 ML Ga sample from wafer 1, where the acceptor (in black) and WL (in red) signals are spectrally well separated (as seen in figure 2(a)) and a 2.2 ML Ga sample from wafer 2 (in blue), where the WL cannot be spectrally well separated by PL measurements (shown in figure 2(b)). Bandpass filters in front of the detector isolated the relevant PL signals. A wavelength range of 825–835 nm was used for the (A^0A^0, e) signal and 840–850 nm for the WL signal in the 1.4 ML Ga sample. A wavelength range of 827–837 nm was used for the signal from the 2.2 ML Ga sample. Exponential decay fitting to the 1.4 ML Ga sample shows that the decay time of (A^0, e) is $\tau_{(A^0,e)} = 13$ ns. This is significantly greater than the WL lifetimes, which are found, by fitting using double exponential decay functions, to be $\tau_{\mathrm{WL_1}} = 0.3$ ns and $\tau_{\mathrm{WL_2}} = 1.2$ ns. The short WL decay time may be due to exciton relaxation to the QD or other losses. Note that the measured 0.3 ns is close to the instrument response time, which is of the order of 0.2 ns. The slower WL decay time is likely to correspond to the recombination of carriers between states in the WL, with the radiative recombination component visible as PL signal. Similar measurements (not shown here) at different positions on wafers 1 and 2, where the WL can be

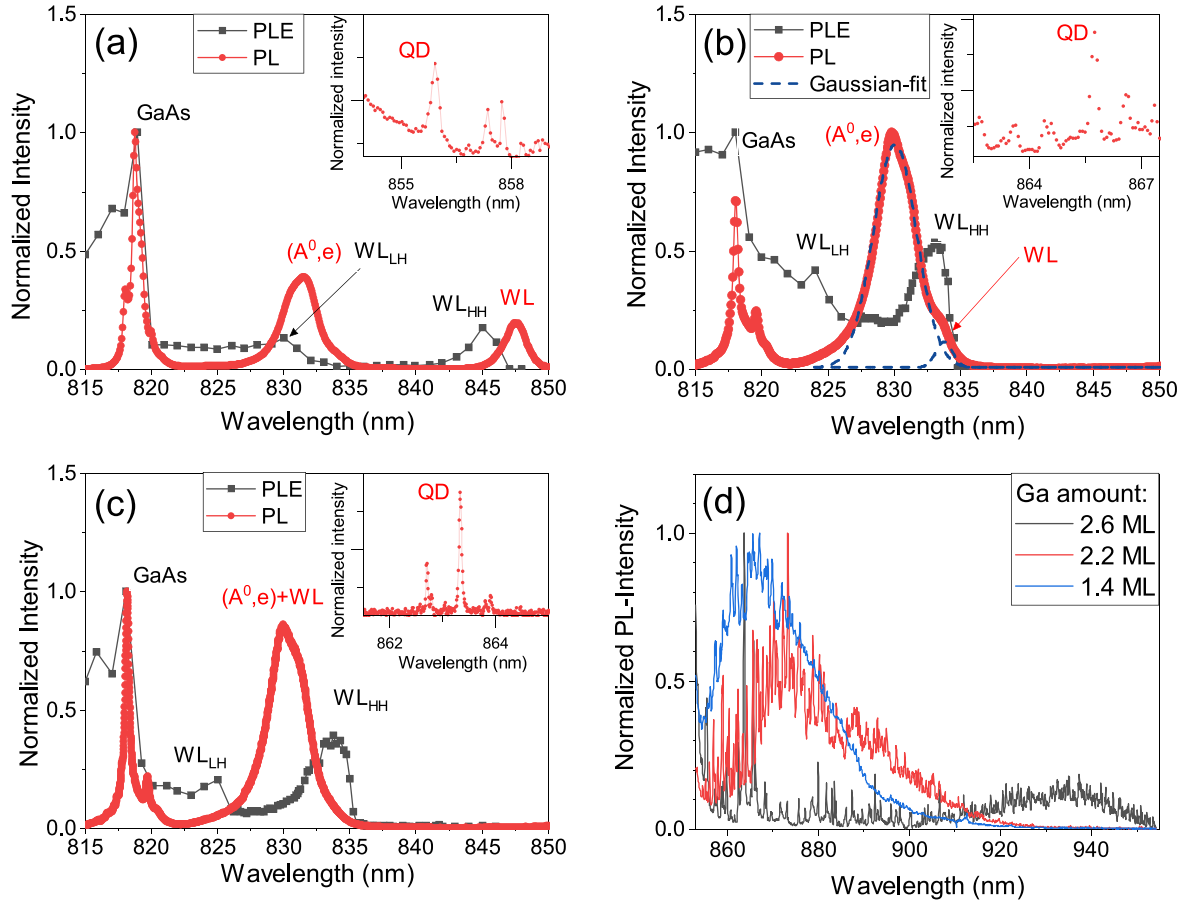

Figure 2. Normalized PL and PLE intensities for spots on wafer 1 with (a) 1.4 ML, (b) 2.2 ML and (c) 2.6 ML of deposited Ga amounts for Ga termination. PL data contains signal from the GaAs free exciton, (A^0, e) and WL radiative recombinations, whereas the PLE data identifies GaAs, WL_{LH} and WL_{HH} states as the sources of charge carriers recombining in a selected QD. The PL of the 'sensor' QD is labeled as 'QD' in the inset of each figure. Other lines in the insets originate from PL of other QDs. (d) Normalized μ-PL spectra of the QDs from the three different positions along the Ga gradient investigated in (a)–(c).

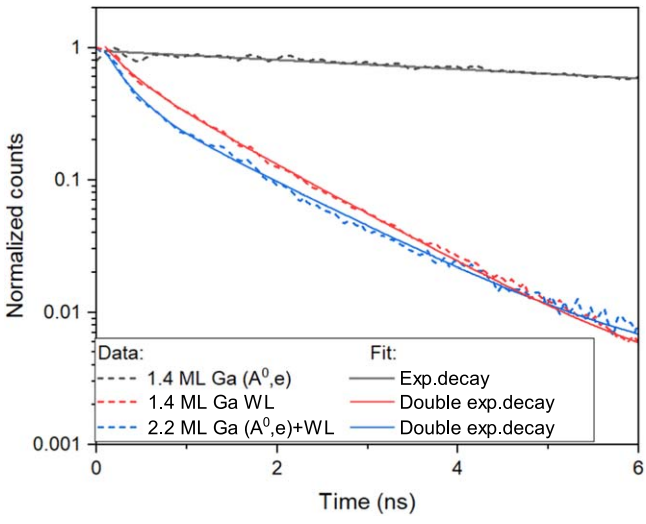

Figure 3. Normalized time resolved photoluminescence for a 1.4 ML Ga sample with spectrally separable (A^0, e) (black) and WL (red) PL signals with corresponding exponential fits and for the 2.2 ML Ga with spectrally overlapping (A^0, e) and WL signals (blue), respectively. The signal that contains WL emission is fitted with a double exponential decay and shows significantly shorter lifetimes than pure (A^0, e) emission.

resolved in the PL spectrum, resulted in lifetimes in the ranges $\tau_{(A^0,e)} = 9 - 13$ ns, $\tau_{WL_1} = 0.2 - 0.6$ ns and $\tau_{WL_2} = 1.2 - 1.8$ ns. It is therefore clear that the WL emission can be distinguished from the acceptor signal due to the significant difference in decay time.

The fitting of a double-exponential decay function to the mixed (A^0, e) and WL emission of the 2.2 ML sample gives $\tau_{Mix_1} = 0.3$ ns and $\tau_{Mix_2} = 1.3$ ns. Both these lifetimes are in the range of lifetimes of the WL recombination determined above. In the mixed state the decay with a long lifetime of the acceptor excitation $\tau_{(A^0,e)}$ (13 ns) contributed much less to the measured signal and was not captured in fitting with two lifetimes. Further TR PL measurements (not shown here) at different positions on wafers 2, where similarly the WL cannot be spectrally well separated by PL measurements result in lifetimes of mixed states in the range $\tau_{Mix_1} = 0.2 - 0.4$ ns and $\tau_{Mix_2} = 1.2 - 1.6$ ns. These values are within the range of decay times for WL emission for Ga deposition below 2.2 ML where the WL emission can be clearly resolved and is one order of magnitude smaller than that for (A^0, e) emission. These observations indicate that, for Ga deposition larger than 2.2 ML, the acceptor peak in the PL is in fact composed of emission from (A^0, e) and the WL.

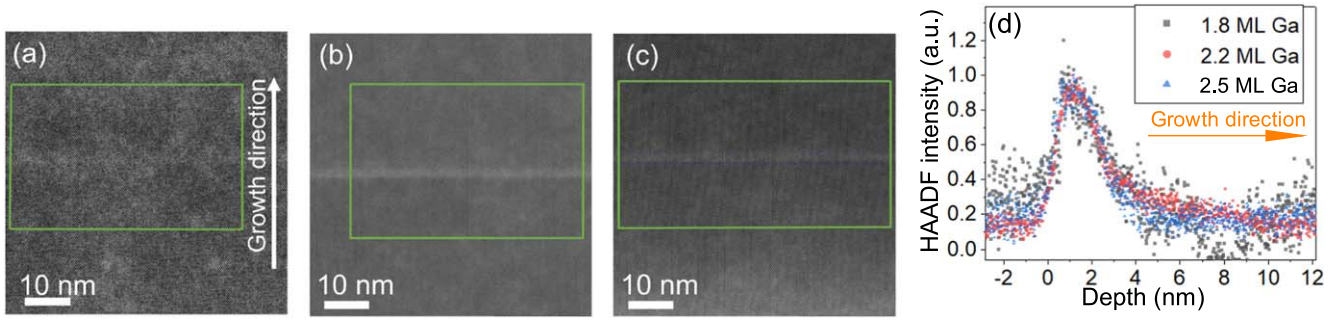

Figure 4. Cross-sectional HAADF STEM images from locations on wafers with (a) 1.8 ML, (b) 2.2 ML and (c) 2.5 ML of deposited Ga amount for Ga-termination. The bright horizontal line in the images indicates a continuous InGaAs layer—the wetting layer. (d) A variation of the HAADF signal intensity along the growth direction (perpendicular to the WL). The signal is an average in the direction parallel to the WL inside the green frames in figures (a)–(c). It is normalized to the maximum intensity.

4.3. TEM

Three samples, with deposited Ga amounts of 1.8 ML Ga, 2.2 ML Ga and 2.5 ML Ga, were investigated with TEM. Both samples with higher deposited Ga amounts are from wafer 2. The STEM imaging conditions were identical in studies of the specimens. HAADF STEM images of the three samples are shown in figures 4(a)–(c). In all three samples, a continuous bright line is observed, indicating a continuous InGaAs WL. The sample with the lowest amount of deposited Ga shows the weakest contrast of the WL relative to the surrounding GaAs. This may be due to a small difference in In deposition amount between wafer 1 and 2 despite having nominally the same amount or because of an artefact from the measurements and TEM lamella preparation. Figure 4(d) shows the normalized line scan intensity (averaged over ∼70 nm along the WL) along the growth direction for all three samples. All distributions show a sharp increase in the In signal at the start of the In deposition. The In segregates during overgrowth with GaAs, giving a more gradual drop in In concentration along the growth direction. This profile can be observed for all three samples. The thicknesses of these WLs are the same for all Ga deposition amounts. Note that the intensity fluctuation in the linescan of the sample with 1.8 ML Ga is above the noise in the TEM measurements.

The data presented here provide strong evidence for the presence of a WL in droplet-epitaxy-grown InAs dots on GaAs substrates, even in the case of Ga-terminated surfaces. This may be due to In exchange with Ga atoms on the Ga-terminated surface, resulting in a partially In-terminated surface during the initial stages of In deposition. During the recrystallization step, this In-Ga-terminated surface would form an InGaAs WL. Alternatively, outdiffusion from the In droplet during the recrystallization step may result in the formation of a thin WL between the dots. This kind of out-diffusion has been observed with GaAs droplets on AlGaAs surfaces, leading to nano-disks with a diameter of up to several 100 nm forming around the dots [14]. We have not seen evidence for this disk formation when carrying out AFM measurements on surface droplet epitaxy dots grown under the conditions investigated here and shown in figures 1(f)–(g). However, given the greater diffusion length of In compared to Ga atoms on GaAs [28, 29], we cannot exclude that this has occurred but that the ring is so large and small in height that it has not been observed in AFM measurements.

5. Conclusions

In this work we have investigated whether the Ga deposition amount prior to In droplet epitaxy can inhibit the formation of a WL. We have demonstrated that the Ga deposition amount prior to In droplet epitaxy is an effective tool to tune the WL emission wavelength. This emission wavelength was reduced until the WL signal overlapped with the GaAs free-electron-acceptor signal in PL measurements, such that these signals could not be spectrally distinguished. However, the presence of WL absorption peaks in PLE unambiguously revealed the WL in all studied Ga amounts. The presence of the WL was also confirmed by time-resolved measurements of the emission decay lifetime and HAADF STEM measurements. These measurements show a clear presence of a WL signal in samples with the investigated Ga depositions amounts from 1.4 to 2.6 ML, and with 1.4 ML of deposited In, both deposited at 350 °C. This is in contrast with a previous report of WL-free InAs droplet epitaxy dots [10]. This may indicate the effect of subtle differences in growth parameters such as chamber background pressure during droplet deposition, As pressure and substrate temperature during droplet recrystallization in different MBE chambers. This work demonstrates the sensitivity of complementary PLE, TR PL and TEM measurements to identify the presence of a WL in the absence of a WL emission signature in photoluminescence measurements.

Acknowledgments

We thank members of the ML4Q Cluster for stimulating discussions and Christoph Krause and Benjamin Bennemann for technical support in growing the sample. Access to the Helmholtz Nano Facility (HNF) and the Ernst Ruska-Centre (ER-C) at Forschungszentrum Jülich is acknowledged. We acknowledge funding from Germany's Excellence

Strategy-Cluster of Excellence Matter and Light for Quantum Computing (ML4Q) EXC 2004/1-390534769.

Data availability statement

The data that support the findings of this study are available upon reasonable request from the authors.

ORCID iDs

D Fricker https://orcid.org/0000-0002-8874-8720
M Lepsa https://orcid.org/0000-0001-7094-7126

References

[1] Becher C, Kiraz A, Michler P, Imamoğlu A, Schoenfeld W V, Petroff P M, Zhang L and Hu E 2001 *Phys. Rev.* B **63** 121312
[2] Leonard D, Pond K and Petroff P M 1994 *Phys. Rev.* B **50** 687
[3] Shields A J 2007 *Nat. Photon.* **1** 215–23
[4] Lodahl P, Mahmoodian S and Stobbe S 2015 *Rev. Mod. Phys.* **87** 347–400
[5] Sanguinetti S, Henini M, Grassi Alessi M, Capizzi M, Frigeri P and Franchi S 1999 *Phys. Rev.* B **60** 8276–83
[6] Seravalli L, Trevisi G, Frigeri P, Franchi S, Geddo M and Guizzetti G 2009 *Nanotechnology* **20** 275703
[7] Wang Q Q, Muller A, Bianucci P, Rossi E, Xue Q K, Takagahara T, Piermarocchi C, MacDonald A H and Shih C K 2005 *Phys. Rev.* B **72** 3
[8] Suzuki T, Singh R, Bayer M, Ludwig A, Wieck A D and Cundiff S T 2018 *Phys. Rev.* B **97** 161301
[9] Löbl M C, Scholz S, Söllner I, Ritzmann J, Denneulin T, Kovács A, Kardynał B E, Wieck A D, Ludwig A and Warburton R J 2019 *Commun. Phys.* **2** 93
[10] Skiba-Szymanska J *et al* 2017 *Phys. Rev. Appl.* **8** 1–8
[11] Sanguinetti S, Watanabe K, Tateno T, Gurioli M, Werner P, Wakaki M and Koguchi N 2003 *J. Cryst. Growth* **253** 71–6
[12] Gurioli M, Wang Z, Rastelli A, Kuroda T and Sanguinetti S 2019 *Nat. Mater.* **18** 799–810
[13] Anderson M, Müller T, Huwer J, Skiba-Szymanska J, Krysa A B, Stevenson R M, Heffernan J, Ritchie D A and Shields A J 2020 *Npj Quantum Inf.* **6** 14
[14] Bietti S, Somaschini C, Esposito L, Fedorov A and Sanguinetti S 2014 *J. Appl. Phys.* **116** 114311
[15] Balakirev S V, Solodovnik M S and Ageev O A 2018 *Phys. Status Solidi (b)* **255** 1700360
[16] Mano T, Watanabe K, Tsukamoto S, Fujioka H, Oshima M and Koguchi N 1999 *Japan. J. Appl. Phys.* **38** L1009–11
[17] Jo M, Mano T and Sakoda K 2011 *Cryst. Growth Des.* **11** 4647–51
[18] Wang L, Rastelli A and Schmidt O G 2006 *J. Appl. Phys.* **100** 064313
[19] Fischione P E, Williams R E, Genç A, Fraser H L, Dunin-Borkowski R E, Luysberg M, Bonifacio C S and Kovács A 2017 *Microsc. Microanal.* **23** 782–93
[20] Kovács A, Schierholz R and Tillmann K 2016 *J. Large-scale Res. Facil.* **2** A43
[21] Kudo K, Makita Y, Takayasu I, Nomura T, Kobayashi T, Izumi T and Matsumori T 1986 *J. Appl. Phys.* **59** 888–91
[22] Bimberg D, Munzel H, Steckenborn A and Christen J 1985 *Phys. Rev.* B **31** 7788
[23] Babiński A, Borysiuk J, Kret S, Czyż M, Golnik A, Raymond S and Wasilewski Z R 2008 *Appl. Phys. Lett.* **92** 171104
[24] Zieliński M *et al* 2015 *Phys. Rev.* B **91** 085303
[25] Brunner K, Abstreiter G, Bohm G, Trankle G and Weimann G 1994 *Phys. Rev. Lett.* **73** 1138
[26] Garro N, Pugh L, Phillips R T, Drouot V, Simmons M Y, Kardynal B and Ritchie D A 1997 *Phys. Rev.* B **55** 13752–60
[27] Moskalenko E S, Karlsson K F, Holtz P O, Monemar B, Schoenfeld W V, Garcia J M and Petroff P M 2002 *Phys. Rev.* B **66** 195332
[28] Wakejima A 1994 *J. Vac. Sci. Technol.* B **12** 1102
[29] Koshiba S, Nakamura Y, Tsuchiya M, Noge H, Kano H, Nagamune Y, Noda T and Sakaki H 1994 *J. Appl. Phys.* **76** 4138–44